A Depth Image Processing Algorithm for Monitoring Product Flow on a Conical Feeder Unit of a Multihead Weigher

Julia Isabel Hartmann[®] and Christoph Ament[®]

Chair of Control Engineering, University of Augsburg, Universitätsstraße 2, 86159 Augsburg, Germany

Keywords: Depth Image Processing, Multihead Weigher, Feeder, Multi-Object Tracking.

Abstract:

Cameras are widely used as sensors in both industrial and research settings for tasks such as quality inspection, measurement, process monitoring, and control. Depending on the application, customized image processing algorithms are required to extract quantitative measurement data from captured images. This paper presents a novel depth image-based data acquisition algorithm for tracking the motion of multiple products on the rotating conical feeder unit of a multihead weigher, an industrial weighing system composed of multiple load cells. The acquired depth image data can be used for the parameter identification and verification of a model, which simulates particle motion on the feeder surface. Future work aims at implementing the image processing algorithm on a programmable logic controller to enable real-time tracking and integration with the control system of the multihead weigher in an industrial environment.

1 INTRODUCTION

In the food industry, multihead weighers are often used to weigh and proportion products to a specific pack size. A multihead weigher represents an industrial scale that enables the simultaneous weighing of several partial amounts through multiple load cells. Moreover, after weighing, the multihead weigher automatically combines a subset of the partial amounts to a favorable weight. Within the multihead weigher, the conical feeder unit is deployed at the beginning of the product flow and distributes the falling products radially outward into the dosing channels that lead over preliminary hoppers to the weighing hoppers and the load cells (see Figure 1). Thus, the feeder has a profound impact on the product distribution among the load cells. The weight distribution among the load cells can, in turn, positively influence the combination process and the precise achievement of the target weight. Furthermore, approaching the target weight as closely as possible corresponds to a minimal product giveaway and, thus, monetary savings.

Several aspects concerning the multihead weigher have been addressed in the literature so far.

Machine topology. The determination of the optimal number of hoppers to be installed in a multi-

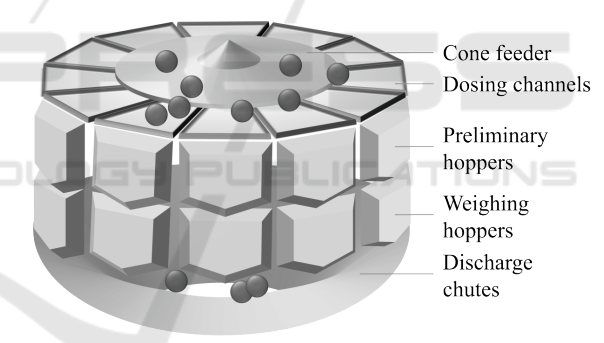


Figure 1: Layout of a multihead weigher.

head weigher has been formulated as a stochastic biobjective design optimization problem. This problem has been addressed using Monte Carlo simulation techniques (van Niekerk et al., 2021).

Hopper setpoints. In each weighing cycle, a predefined quantity of product is allocated to each weighing hopper, governed by its setpoint. To identify the optimal hopper setpoints, various optimization strategies have been applied, including Response Surface Methodology (Beretta and Semeraro, 2012), heuristic approaches (Del Castillo et al., 2017), gradient-based algorithms, brute-force search, and random sampling methods (Beretta et al., 2016). Furthermore, research has been conducted on the use of both uniform and variable setpoints across hopper subgroups (Garcia-Diaz and Pulido-Rojano, 2020).

a https://orcid.org/0009-0003-6848-833X

b https://orcid.org/0000-0002-6396-4355

Subset combination. The selection of the optimal combination of hopper fillings to achieve a total weight that closely matches a specified target is a central problem of the multihead weigher. Various algorithmic approaches have been proposed, including bit-wise operation-based combination algorithms (Keraita and Kim, 2007) and dynamic programming techniques (Imahori et al., 2010; Imahori et al., 2012; Imahori et al., 2014). Bi-objective optimization methods have also been employed to minimize weight variability while simultaneously accounting for the residence time of products in the hoppers (Pulido-Rojano et al., 2015; Pulido Rojano and Garcia Diaz, 2019; Díaz et al., 2017). In systems with a double hopper layer, the packaging process has been formulated as both a single-objective (An et al., 2024; García-Jiménez et al., 2021) and a bi-criteria optimization problem, with solutions developed using dynamic programming (Karuno et al., 2010) and bruteforce search (García-Jiménez et al., 2023). The problem of optimal simultaneous packaging of two products has been addressed using dynamic programming (Imahori et al., 2010; Imahori et al., 2012), while mixture packaging of two different products has been explored using both dynamic programming (Imahori et al., 2014) and a greedy heuristic (Karuno and Nakahama, 2020).

Variability reduction. Variability in the weighing process has been quantitatively assessed using the Percentage Variability Reduction Index (Salicrú et al., 1996; Barreiro et al., 1998). In particular, the impact of specific packaging strategies on variability has been evaluated through a Six Sigma methodology (Pulido-Rojano and Garcia Diaz, 2014). Additionally, modified control charts have been employed to monitor package weights under novel packaging strategies aimed at reducing variability (García-Díaz and Pulido-Rojano, 2017).

Feeder unit modeling. A dynamic friction model with contacts has been proposed to model the motion of a particle on a conical feeder for the viscoelastic case (Hartmann et al., 2023). The model encompasses a specific kinematic model for the conical feeder to constantly calculate the constraint position, velocity, and, thus, forces. Specifically, the overall model is a nonlinear parameter-varying (NLPV) model and its varying parameters have been identified by a multistage optimization approach, considering the varying parameters as functions of the initial position and control input of the system (Hartmann and Ament, 2025).

For the multi-stage parameter identification approach, measurement data is required. Given the nature of the problem, a camera-based sensing solution is considered suitable for capturing the product

flow on the feeder unit. A depth-sensing camera is preferred over a conventional area scan camera, as it enables future extensions of the system for estimating product weight on the feeder. In this paper, an automatic image processing pipeline is proposed to obtain the large dataset required for the identification approach by extracting motion data from the captured images. Furthermore, the image processing algorithm is planned to support process monitoring and control of the feeder unit during operation in the future. The image processing algorithm has been successfully adapted by the authors to operate on color images as well.

This paper is organized as follows. Section 2 describes the hardware setup and the design of experiments. Section 3 details the data acquisition process based on the depth-image processing algorithm. Section 4 presents the extension of the proposed image processing approach to color images. Finally, Section 5 concludes the paper and provides an outlook on future work.

2 HARDWARE AND DESIGN OF EXPERIMENTS

2.1 Hardware Setup

At the University of Augsburg, a demonstrator of the feeder unit with a diameter of 45 cm is available for experimental testing. The demonstrator is an exact replica of the feeder component used in an industrial multihead weigher system. In industrial applications, both rotating and vibrating feeder variants are employed, depending on the type of product being handled. This research project focuses specifically on challenging, sticky products, which are typically conveyed using a rotating cone feeder.

The demonstrator consists of a stepper motor with a gearbox that drives a metal cone feeder, capable of reaching a maximum rotational velocity of $290\,^{\circ}\,\mathrm{s}^{-1}$. For sensing, an Intel RealSense D435 stereo camera is employed. In addition to capturing depth images, the camera provides color images via its integrated RGB module. The depth output supports resolutions



Start marker

Figure 2: Hardware setup with initial placement of the specimen.

up to 1280×720 px and frame rates of up to 90 fps, with a depth accuracy of less than 2% at a distance of 2 m. In addition, the Intel RealSense software development kit (SDK) is compatible with both MATLAB and Python, facilitating integration into the data acquisition and processing pipeline.

The D435 camera is selected for its wide depth field of view $(87^{\circ} \times 58^{\circ})$ and effective range of 0.3 m to 3 m, which allows full coverage of the scene surrounding the feeder without exceeding the spatial constraints of the laboratory setup. The device is mounted directly above the feeder, aligned vertically downward, at a distance of 34.5 cm from the apex of the cone. The height of the cone is 6 cm.

To enhance image quality and avoid reflections, the metal cone is covered with a matte black metal foil. A foil seam running radially outwards from the center to the cone edge is unavoidable, but is used to align the cone with the start marker and to place the specimen in the same position and orientation for each measurement (see Figure 2).

2.2 Experimental Design

A small wooden plate (diameter: 3 cm, height: 1.5 cm, weight: 5.277 g), which is covered by felt on either side, is employed as a specimen. To control the orientation of the specimen, an arrow marks the bottom and angular orientation (see Figure 2).

Each experiment is conducted as follows. First, the feeder foil seam is aligned with the start marker. Then, the specimen is placed onto the foil seam with the arrow pointing downwards. Finally, the depth camera and data recording is started at a resolution of $848 \times 480 \,\mathrm{px}$ and a frame rate of 90 fps and the feeder is driven with a step reference velocity according to the test plan. The reduced resolution is selected because the maximum frame rate of 90 fps cannot be achieved at the highest resolution. Nevertheless, the chosen resolution provides sufficient spatial detail for the task at hand.

As in the parameter identification reference (Hartmann and Ament, 2025), regarding the test plan, a full factorial design is followed, which considers the two explanatory variables motor angular velocity ω and initial distance Δ between the center of the feeder and the centroid of the specimen. The centroid of the specimen is projected onto the cone surface for measuring the initial distance Δ . The target variable is the position of the centroid of the specimen. Five different initial distances Δ_i of 4.5 cm, 7.5 cm, 10.5 cm, 13.5 cm and 16.5 cm are used. Furthermore, the angular velocity of the motor is varied from 100° s⁻¹ to 290° s⁻¹ in steps of 10° s⁻¹

in either rotational direction. Note, that $100^{\circ} \, \mathrm{s}^{-1}$ is selected as the lowest speed because at $100^{\circ} \, \mathrm{s}^{-1}$ the specimen remains at its initial radial position regardless of the initial distance. Finally, each test point is repeated n=3 times. In total, 600 measurements are conducted.

In each experiment, the depth frames of the feeder are captured, processed by means of the hole filling filter of the Intel RealSense SDK, and the angular velocity of the motor and the assigned timestamps are recorded for a predefined recording time. Afterwards, the recorded data are processed offline by the custommade depth image processing algorithm. Hereby, the algorithm can automatically detect multiple objects in a depth frame and assign them to motion tracks through an assignment algorithm. Multiple object and track assignment and handling using an Extended Kalman filter (EKF) is implemented as described in (MathWorks, 2025c; MathWorks, 2025d).

3 DATA ACQUISITION AND IMAGE PROCESSING ALGORITHM

An overview of the depth image processing algorithm is presented in Figure 3. The algorithm comprises five main components. First, a calibration procedure is performed. Subsequently, the necessary processing tools and data structures are initialized. In the next step, the depth frame is preprocessed to enhance object visibility and enable reliable detection. After object detection, the detections are assigned to existing tracks or used to initialize new ones. Finally, all tracks, both active and inactive, are updated according to the current results.

3.1 Calibration

For calibration purposes, a single depth frame showing the empty feeder needs to be captured before or after a measurement series. Based on this frame, a semi-automatic calibration is performed once before all measurements can be processed. At first, the left, right, bottom, and top boundaries of the feeder are defined manually as a rectangle to crop the frame to the size of the feeder. Afterwards, the circular Hough transform is applied to the cropped, sharpened, and grayscale transformed frame to automatically identify the circular boundary of the feeder, its center, and radius. If multiple circles are detected, the circle whose center is closest to the center of the cropped image is selected. If the selected circle is located too far

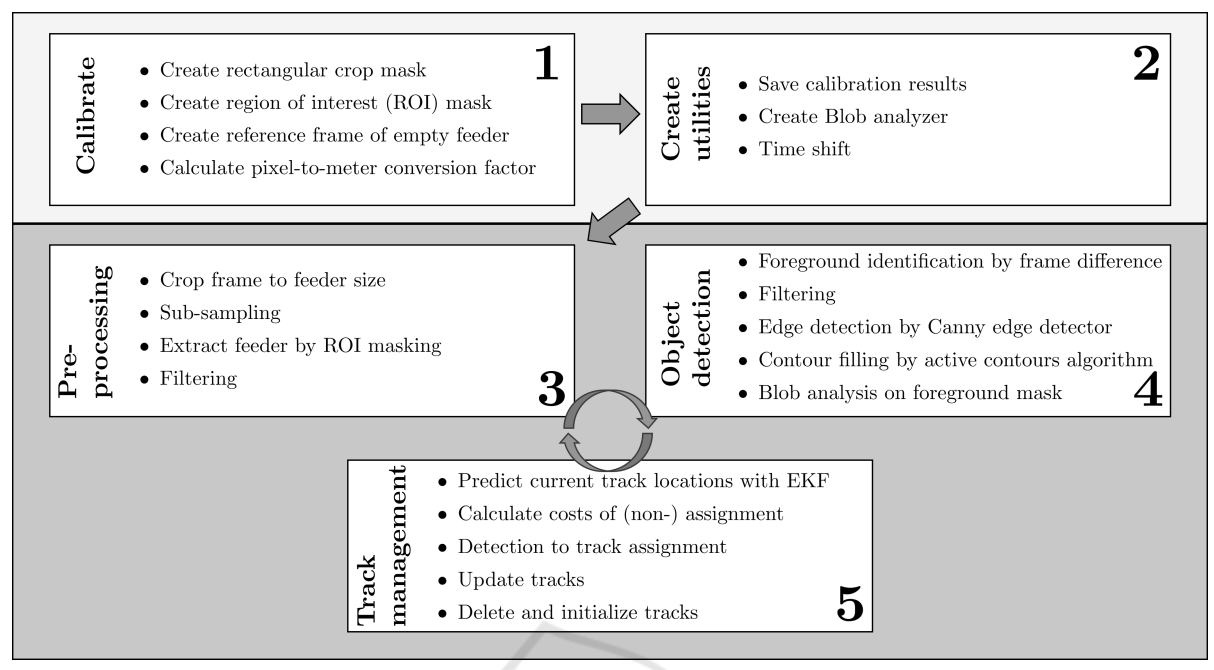


Figure 3: Image processing algorithm.

from the image center or its diameter is significantly smaller than the width of the cropped image, the calibration is considered invalid, and manual calibration is recommended. When a valid circle is identified, a circular region of interest (ROI) mask is generated based on the detected parameters. This mask is subsequently used to isolate the feeder in later stages of the image processing algorithm.

Moreover, for object detection, a reference frame with the depth representation of the empty feeder is necessary. For this purpose, the frame showing the empty feeder is cropped to feeder size, median-filtered to sub-sample and to reduce computational burden, and small image defects, that have not been removed by the initial hole filling of the Intel RealSense SDK hole filling filter, are filled by subsequent morphological image processing operations (dilation with diamond-shaped structuring elements). Next, an edge-preserving filtering using a bilateral filter with Gaussian kernels is performed to smooth the image.

Finally, based on the reference frame, the pixel-tometer conversion factor c_f is calculated with the cone radius r_m in meters and the radius r_{px} of the identified feeder boundary in pixels:

$$c_f = \frac{r_m}{r_{px}}. (1)$$

Figure 4 illustrates the calibration process. Initially, the original frame, which contains defects and irrelevant information outside the conical region, is cropped using the white crop rectangle, as shown in

the first image. The resulting cropped image is depicted in the second panel. Subsequently, the circular boundary of the cone is defined either manually or automatically using a circular Hough transform. The region inside the white circle in the third image marks the region of interest for each frame. Finally, the reference frame obtained after cropping and filtering is presented in the rightmost image.

3.2 Create Utilities

The calibration results are stored as utilities and include the crop rectangle, the center and radius of the feeder in pixels, the ROI mask, the reference frame, and the conversion factor.

Furthermore, a Blob analyzer object with a minimum Blob area of 300 px is needed to identify image regions with similar properties and, thus, to detect objects. It should be noted that the minimum Blob area is dependent on the physical size of the sample and can be estimated in advance based on the image resolution and the area occupied by the sample within the image. In addition, defining a maximum Blob area can be beneficial, as it reduces the number of detected Blobs during object detection, thereby decreasing the computational load by limiting the number of candidates that require further analysis.

Furthermore, the recorded timestamps are shifted to a start time of 0s, to represent the time passed since the start of the recording.

Moreover, empty data structs are initialized for the

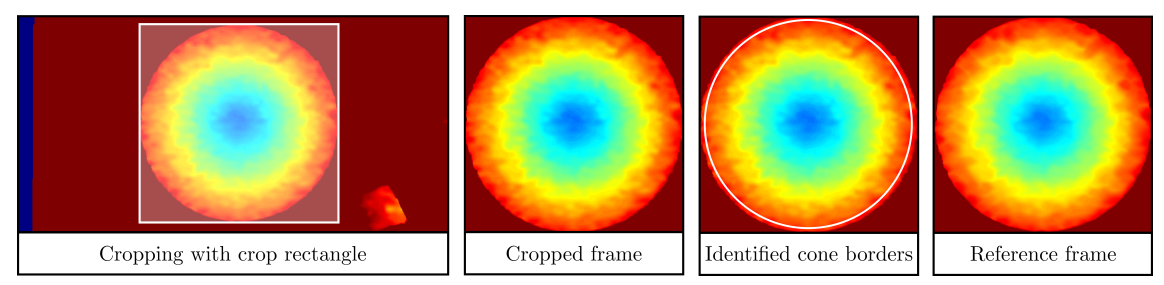


Figure 4: Calibration procedure.

tracks and deleted tracks. Each struct comprises several fields storing information for object tracking:

- id: ID of the track,
- bbox: Current bounding box of the last detection,
- *kalmanFilter:* Kalman filter object for motion-based object tracking,
- age: Number of frames since the track has been initialized,
- *totalVisibleCount:* Number of frames in which detections have been assigned to the track,
- consecutiveInvisibleCount: Number of consecutive frames in which no detections have been assigned to the track,
- *predictedCentroid:* Predicted centroids of the detections of this track,
- assignedCentroids: Centroids of the detections assigned to the track,
- *timeAssignedCentroids:* Time stamps of the detections assigned to the track,
- velocityAssignedCentroids: Rotational velocity of the feeder, when the detection was assigned to the track.

3.3 Preprocessing

From the preprocessing step onward, data are handled frame by frame in a loop. At first, the frame is cropped to feeder size and sub-sampled by a nonzero median filtering. Then, the feeder image part is extracted using the ROI mask. After the Intel Realsense SDK hole filling filter remaining defects in the depth image are filled by morphological dilation and, if necessary, by inserting corresponding depth values of the reference frame of the empty cone. Finally, edge-preserving filtering with Gaussian kernels is performed to smooth the frame. Figure 5 illustrates the preprocessing steps applied to a depth frame. Owing to the advanced filtering capabilities of the Intel RealSense SDK, the initial frame is of generally high quality. A sample object, positioned near the left

boundary of the conical region, is highlighted with a black bounding box. A minor image defect is visible at the left edge of the object. Following region of interest masking and morphological operations, the defect is noticeably reduced. Subsequent application of edge-preserving filtering further smooths and homogenizes the frame, effectively eliminating the defect.

3.4 Object Detection

The challenge in object detection lies in segmenting a frame into the foreground (objects on the feeder) and the background (the feeder itself). For this purpose, a difference frame is calculated by subtracting the reference frame and the currently preprocessed frame. As a result, the difference frame shows the deviation between the two frames, i.e. the foreground and, thus, the objects on the feeder.

Then, the difference frame is refined by excluding negative depth values, noise (very small depth values), and all frame parts beyond the feeder boundary by setting their depth values to 0. Next, a non-zero median filter and an edge-preserving filter are applied to reduce computational burden and enhance image quality. In a subsequent step, the filtered frame is used to detect edges through the Canny edge detector. Afterwards, the active contours (Snakes) region growing technique is used to close the contour and fill it in. Afterwards, small objects and holes are filled in by a morphological opening with a disk-shaped structuring element and a subsequent area opening operation, which removes connected areas with less than a specified pixel size (150 px). The resulting binary mask is the foreground mask of this frame.

Finally, Blob analysis is applied to the foreground mask to find and analyze image areas with similar properties (Blobs), which are the objects here. Then, the identified Blobs are sorted out, in case they are outside the cone boundaries, i.e. the distance between the centroid of the blob and the cone center is larger than the cone radius. Only for the remaining Blobs a coordinate transformation is conducted to shift the feeder center to the origin of the frame coordinate system and to convert the positional values from pixel- to

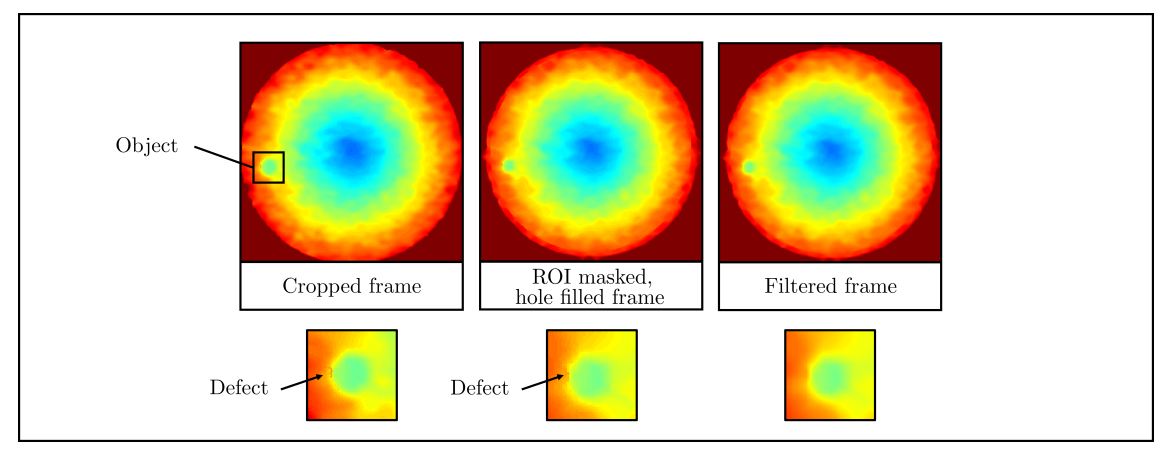


Figure 5: Preprocessing procedure.

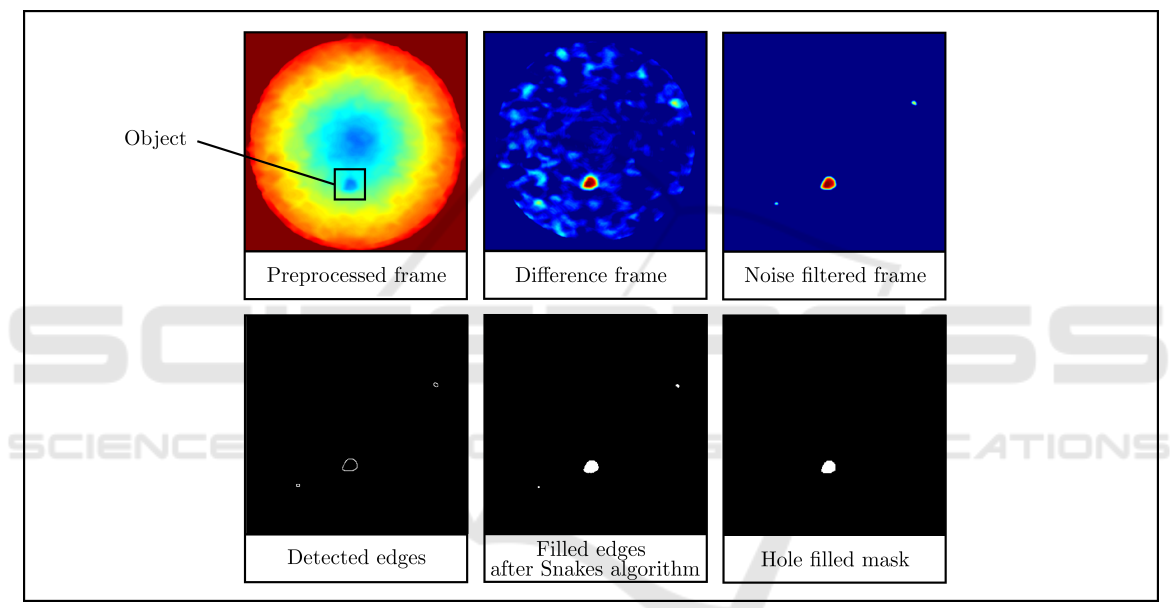


Figure 6: Object detection procedure.

meter-scale. For the subsequent steps, the centroids, bounding boxes, and areas of the Blobs are saved and called *detections* in the following sections.

Figure 6 shows the object detection procedure step by step.

3.5 Track Management

The motion-based multiple object tracking and Kalman filter-based object tracking are described in (MathWorks, 2025c; MathWorks, 2025d) and adopted in this paper. Thereby, the detection to track assignment is enhanced by validity checks that ensure physically reasonable behavior of the objects. The resulting track management process is described in detail next.

Detections need to be assigned to existing or

newly created tracks, and tracks need to be updated or opened accordingly. For this, the current position of all tracks is predicted using an Extended Kalman filter (MathWorks, 2025c). Then, the costs of assigning each detection to each track must be calculated. The costs are calculated based on the distance $d(\mathbf{z})$ between the centroid \mathbf{z} of the detection and the predicted location \mathbf{x} of the track, taking into account the state covariance \mathbf{P} , the measurement noise \mathbf{R} , and the measurement model \mathbf{H} (MathWorks, 2025b)

$$d(\mathbf{z}) = (\mathbf{z} - \mathbf{H}\mathbf{x})^{\top} \Sigma^{-1} (\mathbf{z} - \mathbf{H}\mathbf{x}) + \ln(\det(\Sigma))$$
 (2)

$$\Sigma = \mathbf{H} \mathbf{P} \mathbf{H}^{\top} + \mathbf{R}. \tag{3}$$

Hereby, validity checks are necessary to ensure that a track cannot move inwards towards the feeder center or move faster than the motor speed. To prevent inward movement, the radial positions of the last assigned detection of a track and the current detection are compared. If the radial position of the detection is smaller than the radial position of the track end minus a small offset of 5 cm to compensate for measurement noise, costs are set to a high penalty value of 100. Additionally, detections that would exceed the maximum possible linear velocity $v_{\rm max}$ resulting from the surface velocity of the feeder in either the x- or y-direction, when assigned to a track, incur penalty costs of 100 as well. The maximum possible linear velocity $v_{\rm max}$ is calculated with the feeder rotational velocity ω and the by the third dimension extended current position ${\bf r}=[z_1,z_2,0]$ of the detection

$$v_{\text{max}} = \boldsymbol{\omega} \times \mathbf{r}. \tag{4}$$

Finally, based on the assignment costs and the fixed costs of 95 for non-assignment of a detection, the assignment problem is solved by a variant of the Hungarian assignment algorithm (MathWorks, 2025a) and the assignments and unassigned detections are obtained. After this, the assigned tracks are updated with the centroids of the assigned detections, the current angular velocity of the feeder, and the timestamp. In addition, the correction step of the Extended Kalman Filter is performed using the new detection, while the age counter and total visible count of the tracks are updated by 1 to monitor track lifespan and visibility. The unassigned tracks need to be updated as well by increasing their age and consecutive invisible count by 1. A track is terminated and removed if it has not been assigned a detection for more than 20 frames, or if its visibility, defined as the ratio of the number of frames in which it was visible to its total age, falls below a predefined threshold of 60 %. Once deleted, no further detections can be assigned to the track. (MathWorks, 2025c)

Lastly, for each unassigned detection, a new track is created and an Extended Kalman filter object is initialized. For this purpose, a MATLAB Tracking Extended Kalman filter is used with a constant angular velocity model. The filter states are the position r_x in the x-direction and the y-direction r_y in meters, the velocity v_x in x-direction and y-direction v_{y} in meters per second, and the angular velocity ω in degree per second: $\mathbf{x} = (r_x, v_x, r_y, v_y, \omega)$. A measurement corresponds to the position \mathbf{r} of the particle in all three spatial dimensions. z-position r_z is needed for evaluating a cross product in the subsequent steps. The state covariance is choto $\mathbf{P} = \text{diag}(0.01, 1, 0.01, 1, 0.01),$ sen the process noise to diag(100, 0.01, 100, 0.01, 0.002), and the measurement noise to $\mathbf{R} = \text{diag} (100, 100, 100)$.

3.6 Multi-Object Tracking

Besides tests on a single specimen, the image processing algorithm is evaluated using three samples of similar type. The results of one experiment are presented in Figure 7. Each color represents a track, with three tracks identified in total. Solid lines denote the detections assigned to a track, while lighter-colored plus signs indicate the corresponding Kalman filter predictions. Each sample starts from a different initial position and exhibits either predominantly sticking (blue) or sliding (green, red) behavior. The results confirm that the algorithm successfully identified and maintained three distinct tracks, each corresponding to a specimen. The predictions closely follow the observed motion and persist beyond the last detection, until the track is formally terminated. This continued prediction appears consistent with the expected object dynamics. However, for samples with varying size or shape, the parameters of the Blob analysis and filtering must be adapted to reliably distinguish valid objects from noise. Additionally, scenarios involving overlapping objects remain untested and present a direction for future work.

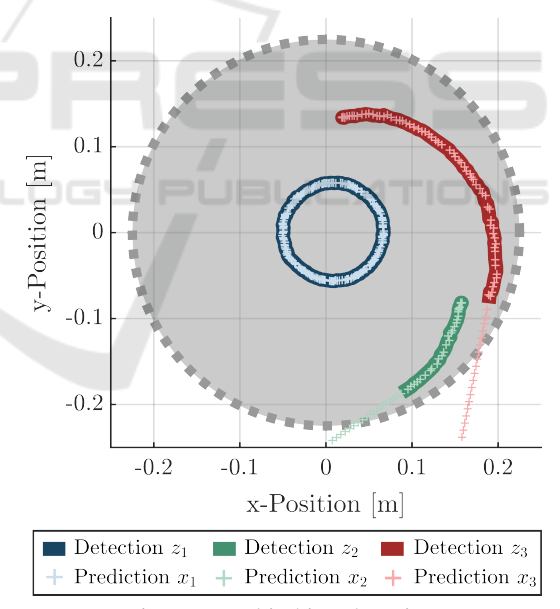


Figure 7: Multi-object detection.

3.7 Detection of Different Objects

Although a round specimen is selected as the primary object for this study, the tracking algorithm is not limited to spherical or circular shapes. To evaluate its generalizability, several static snapshots are acquired using objects of varying shapes, surface materials, and heights. The test specimens include food

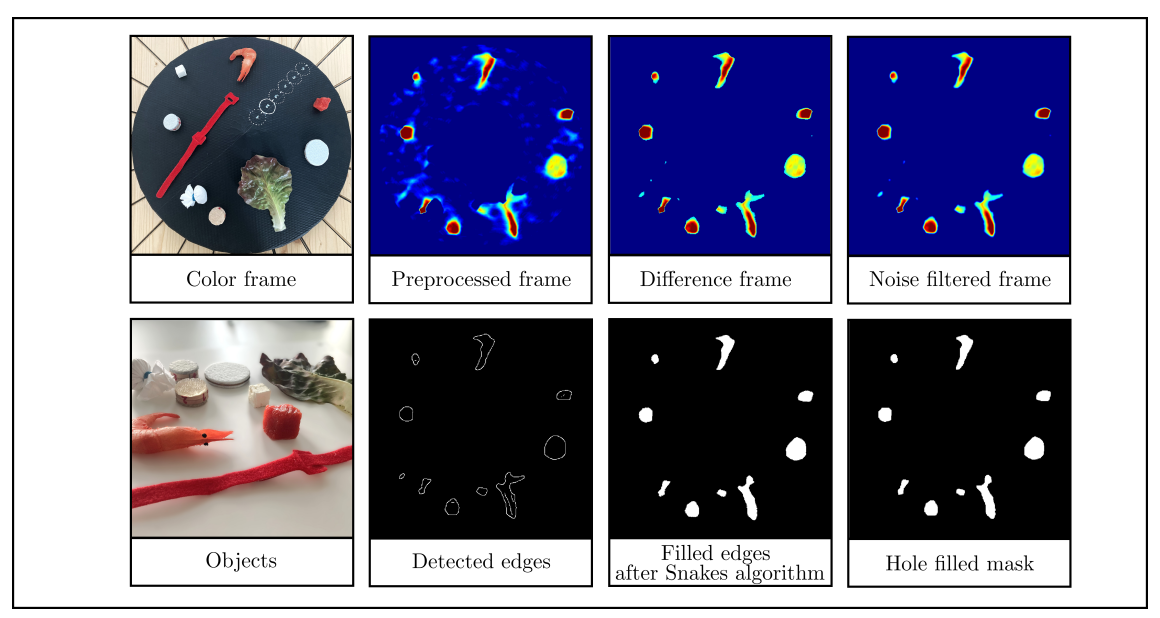


Figure 8: Object detection procedure for different objects.

dummies resembling a salad leaf, a shrimp, a piece of meat, and a piece of feta cheese. Additionally, wooden plates of different diameter, height, and surface material, a small rice-filled bag, and a thin strip of Velcro fastener tape are tested. As shown in Figure 8, all objects except for the thin Velcro fastener tape are successfully detected. However, limitations arise when the object thickness is too small, as observed for the Velcro tape and the salad leaf. In particular, the salad leaf is no longer detected as a single coherent object.

4 EXTENSION TO COLOR IMAGES

An adapted version of the proposed image processing algorithm was also evaluated using color images. This section outlines the necessary modifications required to enable its application in the color image domain.

Calibration. In contrast to the depth image setup, calibration for color images is more straightforward, as no reference frame needs to be acquired. The region of interest mask is generated by identifying the boundary of the cone feeder using circular Hough transform applied to the binarized grayscale version of the color image. The crop mask and the pixel-tometer conversion are determined analogously to the depth image procedure.

Create utilities. The process of creating the utilities remains unchanged.

Preprocessing. The preprocessing pipeline begins

by cropping the input image based on the defined crop rectangle, followed by conversion of the cropped color image to grayscale. The grayscale image is then binarized, and the resulting binary image is masked using the ROI mask. In initial tests, no additional filtering was required, as the preprocessing output was already of sufficient quality.

Object detection and tracking. Object detection is carried out using Blob analysis on the preprocessed binary frame. No further filtering or edge detection is needed.

Track management. The track management logic remains the same as in the original algorithm developed for depth images.

5 CONCLUSION

This paper presented an image processing algorithm for multi-object tracking in depth images, specifically designed for the application with a cone feeder of a multihead weigher. The proposed method demonstrates the feasibility of accurate offline object tracking and measurement data acquisition using a low-cost, consumer-grade stereo camera. Additionally, a pathway for extending the approach to color image processing was outlined, enabling broader applicability.

Despite the favorable price-performance ratio of the selected hardware, particularly regarding resolution and frame rate, several technical limitations remain. These include non-deterministic frame arrival, misordered timestamps, and the absence of a GigE Vision interface, all of which currently restrict real-time integration with a programmable logic controller. Moreover, the Intel RealSense depth camera, being a consumer-grade device, provides only limited depth accuracy (less than 2% at a distance of 2 m). In this study, it is employed for a preliminary feasibility assessment of depth-based motion tracking rather than for precise absolute height measurements. For the intended application, high depth accuracy is not critical, provided that the target objects are sufficiently elevated to be reliably distinguished from the feeder surface.

Due to the constraints of the research project, a comparative evaluation with industrial-grade depth cameras or stereo vision systems in terms of speed, accuracy, and reliability was not feasible, as only the Intel RealSense depth camera was available for investigation.

Nevertheless, the approach establishes a solid foundation for future applications and developments. The image processing algorithm is currently being utilized for automatic parameter identification of a nonlinear model describing particle dynamics on the conical feeder, as demonstrated in (Hartmann and Ament, 2025). Future work will focus on enabling vision-based real-time control of the feeder unit. This will require more sophisticated camera hardware equipped with a GigE Vision interface to ensure deterministic data transmission and real-time compatibility with programmable logic controllers. Additionally, porting the image processing algorithm to an embedded programmable logic controller environment is a necessary step toward industrial deployment.

Further research will explore automatic product identification during the operation of the multihead weigher. By leveraging depth data, projected object area, and estimated material density, the method also offers the potential for approximating the weight of individual items. This capability could improve the dynamic distribution of product weight into individual hoppers, ultimately contributing to more efficient and adaptive packaging processes.

ACKNOWLEDGEMENTS

This work is part of the project "KiKO.BD - KI-Kombinationswaage mittels Big Data" of the programme "BayVFP Förderlinie Digitalisierung" of Bavarian Ministry of Economic Affairs, Regional Development and Energy.

REFERENCES

- An, P., Hong, C.-J., Ri, R.-Y., Yu, C.-J., and O, C.-J. (2024). An improved single objective optimization approach for double-layered multi-head weighing process. *Mathematical Modelling and Applications*, 9(3):61–69.
- Barreiro, J. J., González, C., and Salicrú, M. (1998). Optimization of multiweighing packing proceedings. *Top*, 6(1):37–44.
- Beretta, A. and Semeraro, Q. (2012). On a rsm approach to the multihead weigher configuration. In Volume 1: Advanced Computational Mechanics; Advanced Simulation-Based Engineering Sciences; Virtual and Augmented Reality; Applied Solid Mechanics and Material Processing; Dynamical Systems and Control, pages 225–233. American Society of Mechanical Engineers.
- Beretta, A., Semeraro, Q., and Del Castillo, E. (2016). On the multihead weigher machine setup problem. *Packaging Technology and Science*, 29(3):175–188.
- Del Castillo, E., Beretta, A., and Semeraro, Q. (2017). Optimal setup of a multihead weighing machine. *European Journal of Operational Research*, 259(1):384–393.
- Díaz, J. C. G., Rojano, A. P., and Bosch, V. G. (2017). Bi-objective optimisation of a multihead weighing process. *European J. of Industrial Engineering*, 11(3):403.
- García-Díaz, J. C. and Pulido-Rojano, A. (2017). Monitoring and control of the multihead weighing process through a modified control chart. DYNA, 84(200):135–142.
- Garcia-Diaz, J. C. and Pulido-Rojano, A. D. (2020). Performance analysis and optimisation of new strategies for the setup of a multihead weighing process. *European J. of Industrial Engineering*, 14(1):58–84.
- García-Jiménez, R., García-Díaz, J. C., and Pulido-Rojano, A. D. (2021). Packaging process optimization in multihead weighers with double-layered upright and diagonal systems. *Mathematics*, 9(9):1039.
- García-Jiménez, R., García-Díaz, J. C., and Pulido-Rojano, A. D. (2023). Bicriteria food packaging process optimization in double-layered upright and diagonal multihead weighers. *Journal of Computational and Ap*plied Mathematics, 428:115168.
- Hartmann, J. I. and Ament, C. (2025). Automatic parameter identification of a nonlinear parameter-varying model for a rotating cone feeder [accepted]. In *IEEE/IFAC 9th International Conference on Control Automation and Diagnosis (ICCAD'25)*.
- Hartmann, J. I., Olbrich, M., Hamann, M., and Ament, C. (2023). Simulation of particle motion on rotating cone feeder for a multihead weigher based on dynamic friction modeling. In 2023 IEEE/ASME International Conference on Advanced Intelligent Mechatronics (AIM), pages 138–143. IEEE.
- Imahori, S., Karuno, Y., Nishizaki, R., and Yoshimoto, Y. (2012). Duplex and quasi-duplex operations in automated food packing systems. In 2012 IEEE/SICE

- International Symposium on System Integration (SII), pages 810–815. IEEE.
- Imahori, S., Karuno, Y., and Tateishi, K. (2014). Dynamic programming algorithms for producing food mixture packages by automatic combination weighers. *Journal of Advanced Mechanical Design, Systems, and Manufacturing*, 8(5):JAMDSM0065–JAMDSM0065.
- Imahori, S., Karuno, Y., and Yoshimoto, Y. (2010). Dynamic programming algorithms for duplex food packing problems. In 2010 8th IEEE International Conference on Industrial Informatics, pages 857–862. IEEE.
- Karuno, Y., Nagamochi, H., and Wang, X. (2010). Optimization problems and algorithms in double-layered food packing systems. *Journal of Advanced Mechanical Design, Systems, and Manufacturing*, 4(3):605–615.
- Karuno, Y. and Nakahama, O. (2020). An improved performance of greedy heuristic solutions for a bicriteria mixture packaging problem of two types of items with bounded weights. *Journal of Advanced Mechanical Design, Systems, and Manufacturing*, 14(5):JAMDSM0066–JAMDSM0066.
- Keraita, J. N. and Kim, K. H. (2007). A weighing algorithm for multihead weighers. *International Journal of Precision Engineering and Manufacturing*, 8(1):21–26.
- MathWorks (2025a). assigndetectionstotracks assign detections to tracks for multiobject tracking. https://de.mathworks.com/help/vision/ref/assign detectionstotracks.html, 17.05.2025.
- MathWorks (2025b). distance confidence value of measurement. https://de.mathworks.com/help/vision/ref/vision.kalmanfilter.distance.html, 17.05.2025.
- MathWorks (2025c). Motion-based multiple object tracking. https://de.mathworks.com/help/vision/ug/motion-based-multiple-object-tracking.html, 15.01.2025.
- MathWorks (2025d). Use kalman filter for object tracking. https://de.mathworks.com/help/vision/ug/using-kalman-filter-for-object-tracking.html, 15.01.2025.
- Pulido Rojano, A. and Garcia Diaz, J. C. (2019). Optimisation algorithms for improvement of a multihead weighing process. *International Journal of Productivity and Quality Management*, 1(1):1.
- Pulido-Rojano, A., Garcia-Diaz, J. C., and Giner-Bosch, V. (2015). A multiobjective approach for optimization of the multihead weighing process. In 2015 International Conference on Industrial Engineering and Systems Management (IESM), pages 426–434. IEEE.
- Pulido-Rojano, A. D. and Garcia Diaz, J. C. (2014). Optimization of multihead weighing process using the taguchi loss function. In 8th International Conference on Industrial Engineering and Industrial Management XX International Conference on Industrial Engineering and Operations Management International IIE Conference 2014, pages 305–312.
- Salicrú, M., González, C., and Barreiro, J. J. (1996). Variability reduction with multiweighing proceedings. *Top*, 4(2):319–329.
- van Niekerk, J. E., van Vuuren, J. H., and Lindner, B. G. (2021). Optimizing the number of hoppers on a multi-

head weighing machine. *Journal of Industrial and Production Engineering*, 38(6):401–413.